A comparison of land surface model soil hydraulic properties estimated by inverse modeling and pedotransfer functions

Ethan D. Gutmann[1] and Eric E. Small[1]

Received 27 April 2006; revised 25 October 2006; accepted 8 January 2007; published 10 May 2007.

[1] Soil hydraulic properties (SHPs) regulate the movement of water in the soil. This in turn plays an important role in the water and energy cycles at the land surface. At present, SHPs are commonly defined by a simple pedotransfer function from soil texture class, but SHPs vary more within a texture class than between classes. To examine the impact of using soil texture class to predict SHPs, we run the Noah land surface model for a wide variety of measured SHPs. We find that across a range of vegetation cover (5–80% cover) and climates (250–900 mm mean annual precipitation), soil texture class only explains 5% of the variance expected from the real distribution of SHPs. We then show that modifying SHPs can drastically improve model performance. We compare two methods of estimating SHPs: (1) inverse modeling and (2) soil texture class. Compared to texture class, inverse modeling reduces errors between measured and modeled latent heat flux from 88 to 28 W/m^2. Additionally we find that with increasing vegetation cover the importance of SHPs decreases and that the van Genuchten m parameter becomes less important, while the saturated conductivity becomes more important.

Citation: Gutmann, E. D., and E. E. Small (2007), A comparison of land surface model soil hydraulic properties estimated by inverse modeling and pedotransfer functions, *Water Resour. Res.*, *43*, W05418, doi:10.1029/2006WR005135.

1. Introduction

[2] Soil hydraulic properties (SHPs) play a critical role in land surface models (LSMs). SHPs define the relationship between soil moisture (θ), hydraulic head (ψ), and hydraulic conductivity (K), thus controlling how water moves through the soil. This movement controls the water balance partitioning between evapotranspiration and runoff. In addition, the availability of soil moisture at different depths in the soil column controls the partitioning of two key energy fluxes of concern in climate models, latent and sensible heat. The distribution of soil moisture also controls the partitioning between evaporation and transpiration which has implications for carbon cycling.

[3] LSMs have evolved substantially in the last 30 years, both in physics and numerical techniques. Here, we focus on the hydrology component of LSMs, which has evolved from a single-layer "bucket" model [*Manabe*, 1969] to a multilayer solution to the Richards equation [*Dickinson et al.*, 1993; *Mahrt and Ek*, 1984; *Sellers et al.*, 1986]. More recently, the focus has shifted toward "greening" LSMs by including complex vegetation components [e.g., *Sellers et al.*, 1986; *Bonan et al.*, 2003]. These models have been criticized for the discrepancy between the complexity of aboveground processes, and the simplicity of below-ground processes [*Pitman*, 2003]. Researchers have continued to refine the hydrology submodel of LSMs by refining the representation of groundwater [*Liang et al.*, 2003; *Maxwell and Miller*, 2005; *Yeh and Eltahir*, 2005]. As the parameterization of hydrologic processes becomes more complex, the importance of accurately identifying SHPs will increase. *Pitman* [2003] targets the improvement of hydrologic processes in LSMs as one of the key challenges for future work, and comments on the need for global data sets of SHPs.

[4] Numerous methods have been developed for the measurement of SHPs, but most are time-consuming and expensive [*Stolte et al.*, 1994]. For this reason, pedotransfer functions (PTFs) have been developed to translate more readily available soil texture data or soil texture class into SHPs [*Wosten et al.*, 2001]. *Soet and Stricker* [2003] note substantial variability between SHPs derived using different PTFs. In addition, none of the PTFs tested captured the variability measured in the field. This suggests that the relationship between SHPs and soil texture may not be very strong.

[5] In most LSMs, simple PTFs are used to estimate SHPs according to soil texture class [e.g., *Dickinson et al.*, 1993; *Chen and Dudhia*, 2001]. This approach is popular because it is easy to implement, and because global maps of soil texture class exist. This approach is based on the assumption that there is a one to one mapping between soil texture class and SHPs. However, there is little evidence that this is the case. Indeed, there appears to be more variability of many SHP parameters, such as the van Genuchten m [*van Genuchten*, 1980] and saturated conductivity, within a soil texture class than there is between classes (Figure 1). For example, the saturated conductivity varies from $10^{0.9}$ cm/d to $10^{2.3}$ cm/d ($\mu \pm 1\sigma$) in the sandy loam class, while the texture class mean saturated

[1]Department of Geological Sciences, University of Colorado, Boulder, Colorado, USA.

0043-1397/07/2006WR005135$09.00

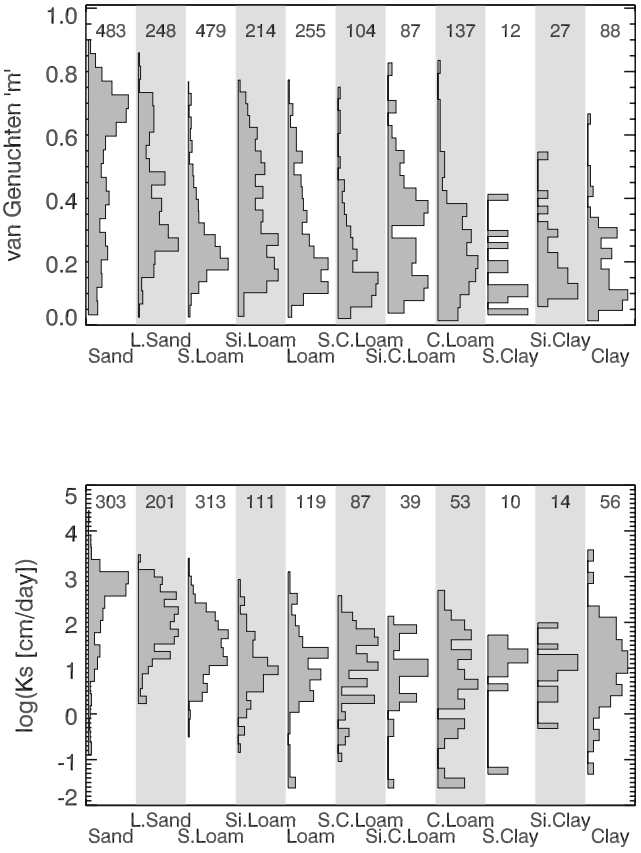

Figure 1. Histograms showing (top) the variability of van Genuchten m parameter and (bottom) the saturated conductivity (Ks) within each soil texture class. Histograms are normalized to have the same maximum height regardless of the number of soils. Numbers on top are the number of samples used in each class. The silt class is not listed because no silts with measured Ks exist in the database.

conductivity generally varies from $10^{0.9}$ cm/d to $10^{1.6}$ cm/d ($\mu \pm 1\sigma$) across all classes.

[6] The scale at which SHPs are defined also presents a problem to land surface modeling [*Feddes et al.*, 1993; *Kabat et al.*, 1997; *Sridhar et al.*, 2003; *Zhu and Mohanty*, 2003; *Braud et al.*, 2005]. Field and laboratory estimates of SHPs are typically made over an area around 100 cm^2. However, LSMs often simulate processes over 100 km^2 areas and larger. LSM scale SHPs must effectively incorporate all of the variability in SHPs within a grid cell, in addition to accounting for effects that do not occur at the scale SHPs are typically measured. For example, within a single grid cell there may be macropores, calcite horizons, bedrock outcrops, substantial topography, and other features which are not accounted for with current SHP models. All SHPs are calibration parameters, for example, lab measurements of moisture content, flow rates, and water potential are used to determine van Genuchten m, α, and K_s that minimize errors between models and measurements. Likewise, SHPs used in LSMs are often thought of as calibration parameters. As a result, relating LSM SHPs to soil texture based on lab SHPs becomes less meaningful. However, inverse modeling is well suited to estimating SHPs that are consistent with the LSM.

[7] The uncertainty in determining SHPs from texture requires the land surface modeling community to question the use of soil texture class as a proxy for SHPs. To determine the error associated with using soil texture class as a proxy for SHPs, we need to know the effect SHPs have on model output. To that end we examine output from the Noah LSM [*Chen and Dudhia*, 2001; *Ek et al.*, 2003] when run with a variety of SHPs from a large database of SHPs. We then compare these model results to model output when run with the average SHPs for a given soil texture class. Earlier work by the authors [*Gutmann and Small*, 2005] showed that soil hydraulic properties had a large impact on model performance in a semiarid grassland with little or no vegetation cover, and that soil texture class was a very poor predictor of SHPs. The current work examines the response of the Noah model across a gradient of mean annual precipitation and vegetation covers. Furthermore, we quantify the degree to which SHP inverse modeling techniques can improve LSM output. Inverse modeling is the process of selecting optimal model parameters so that the model matches a set of measurements. This has the potential to provide a global map of SHPs to be used in LSMs by utilizing remotely sensed measurements.

[8] The results of inverse modeling of SHPs in LSMs may be substantially impacted by vegetation cover. Parameter sensitivity studies [e.g., *Bastidas et al.*, 1999; *Liang and Guo*, 2003] suggest that SHPs and vegetation properties are the most important parameters in LSMs. Vegetation transpiration allows water to be removed from deeper layers in the soil column than bare soil evaporation does [*Chen and Dudhia*, 2001]. This is likely to decrease the model variability related to SHPs because the main impact of SHPs is on the distribution of water within the soil column. If vegetation does decrease the impact of SHPs then inverse modeling of SHPs will be less precise in areas with more vegetation cover. To examine the effects of vegetation, we analyze the model variability related to SHPs as we systematically vary vegetation cover.

[9] To test the effect of SHPs on LSMs we ran three model experiments to answer three questions. (1) What is the range of LH expected given the distribution of SHPs, and how well do soil texture class SHPs predict this LH distribution? This question is important because the answer will examine how well current methods of determining SHPs in LSMs works. (2) How does measured LH compare to modeled LH when using best fit SHPs from inverse modeling, and when using soil texture class average SHPs? This question is important because the answer will demonstrate how well the models are capable of fitting measured data if correct parameters are chosen, as well as further analyzing how well current methods work. (3) Does the model sensitivity to SHPs change with increasing vegetation cover? This question is important because the answer will provide guidance to future researchers on the circumstances required to select SHPs via inverse modeling.

2. Methods

2.1. Soils Database

[10] We used the SHP database of *Schaap and Leij* [1998] as input for this study. This database is a collection of 3 other databases (RAWLS, AHUJA, and UNSODA), and as

such it is one of the largest SHP databases available. The public domain UNSODA database [*Leij et al.*, 1996] forms the bulk of the *Schaap and Leij* [1998] database. The database of *Schaap and Leij* [1998] contains 1306 soils with complete SHP measurements and an additional 825 soils that lack saturated conductivity data. Additionally, this database forms the basis of the widely used US Department of Agriculture Agricultural Research Service's ROSETTA model [*Schaap et al.*, 2001]. Compared to the larger soils database used by *Carsel and Parrish* [1988], which does not contain SHPs, this database is biased toward coarser textured soils. The database of *Schaap and Leij* [1998] contains 253 sands and but only 60 clays, as compared to 803 sands and 1177 clays in the work of *Carsel and Parrish* [1988]. Despite this bias the SHP database is large enough to depict the distribution of SHPs within each texture class, only three soil texture classes are represented by fewer than 50 soils. We used this database because of its international nature, availability of the database to other researchers, as well as the extensive use of this database and the UNSODA database [*Leij et al.*, 1997; *Kravchenko and Zhang*, 1998; *Arya et al.*, 1999; *Hoffmann-Riem et al.*, 1999; *Poulsen et al.*, 2000; *Schaap et al.*, 2001].

[11] The SHPs in this database were not measured at the LSM scale, but it is the best database available. It is based on lab and field measurements of relatively small soil samples that would cover an area of approximately 100 cm^2. These are likely to show more variation in SHPs than would be seen in SHPs derived at the larger scales used in LSMs (0.1–1000 km^2). The Model Parameter Estimation Experiment (MOPEX) [*Duan et al.*, 2006] may generate a database of SHPs at the LSM scale, but currently no such database exists, and existing methods of scaling SHPs from small scale measurement to LSM scales require multiple SHP measurements from the same location [*Zhu and Mohanty*, 2002, 2003]. Their work on SHP scaling also suggests that if an area with homogenous SHPs exists, the small-scale measurement would be appropriate to use at the larger scale. As a result, this database represents a reasonable source of information to test the effect of variation in SHPs.

2.2. Soil Hydraulic Property Model

[12] Many SHP models exist to estimate the relationship between soil moisture, hydraulic conductivity, and hydraulic head. The SHP database of Schaap and Leij uses the van Genuchten model. Translating between SHP models is imperfect [e.g., *Morel-Seytoux et al.*, 1996]; therefore we used the soil hydraulic property model of *van Genuchten* [1980] (equations (1) and (2)).

$$\psi = \left(S^{-\frac{1}{m}} - 1\right)^{\frac{1}{n}} / \alpha \tag{1}$$

$$K = K_s * S^{0.5} * \left(1 - \left[1 - S^{\frac{1}{m}}\right]^m\right)^2 \tag{2}$$

where $S = \frac{\theta - \theta_r}{\theta_s - \theta_r}$, θ = soil moisture content, θ_r = residual moisture content, θ_s = saturated moisture content, K_s is the saturated hydraulic conductivity, and α, n, and m are curve fitting parameters. The parameter space for this model is commonly limited by setting $m = 1 - \frac{1}{n}$, and we also adopt this convention. Residual moisture content is the moisture content at which water ceases to flow through the soil, except by vapor diffusion, and is typically much lower than the wilting point.

[13] Currently, most LSMs use the Campbell [*Campbell*, 1974] SHP model (equations (3) and (4)).

$$\psi = \psi_s \left(\frac{\theta}{\theta_s}\right)^{-b} \tag{3}$$

$$K = K_s \left(\frac{\theta}{\theta_s}\right)^{2b+3} \tag{4}$$

where ψ_s and b are curve fitting parameters, ψ_s is similar to $\frac{1}{\alpha}$ and b is related to n. ψ_s and α are both related to the air entry pressure of the soil, while b and n are related to the pore size distribution. The Campbell model was modified by *Clapp and Hornberger* [1978] and is often cited as such even without modification. The Campbell model is simpler than the van Genuchten model, but it has several limitations. It contains a discontinuity at ψ_s, intended to reflect a single air entry pressure. However, in real soils, a range of pore sizes exist, and as a result, measured data typically vary continuously in this region. In addition, the model discontinuity can introduce numerical problems both in fitting measured data [*Milly*, 1987] and in using it in hydrologic models [*van Genuchten*, 1980]. Furthermore, applying scaling techniques to this type of model has proven more difficult than for others [*Zhu and Mohanty*, 2003]. The van Genuchten model has been shown to fit measured data better than Campbell type models [*Milly*, 1987; *Leij et al.*, 1997], and scaling procedures are available for it [*Zhu and Mohanty*, 2003].

2.3. Land Surface Model

[14] We used the Noah [*Chen and Dudhia*, 2001; *Ek et al.*, 2003] land surface model to examine the effects of SHPs on LSM fluxes. Noah is based on the OSU land surface model [*Mahrt and Ek*, 1984]. The soil hydrologic component of the model solves the diffusion form of the Richards equation in one dimension and we used the *van Genuchten* [1980] model for the relation between hydraulic head, moisture content, and hydraulic conductivity. The fluxes at the land surface are determined to conserve both mass and energy based on a Penman type combination equation. The Noah model is designed to be coupled with the weather research and forecasting model (WRF), but also has an off-line mode in which it can use atmospheric boundary conditions measured near the ground surface. We used the off-line mode here.

[15] The standard Noah model uses the Campbell SHP model [*Campbell*, 1974], but for the reasons outlined in the previous section we modified Noah to use the van Genuchten formulation [*van Genuchten*, 1980]. The Noah model uses a separate subroutine to calculate SHPs, as such, it is possible to test the new subroutine separately from the rest of the model to insure correctness. *Shao and Irannejad* [1999] showed that the specific SHP model used in an LSM does not dramatically alter the LSM, and that if the correct SHPs are chosen, two otherwise identical LSMs with differing SHP models can produce the same output ($r^2 = 0.99$). *Shao and*

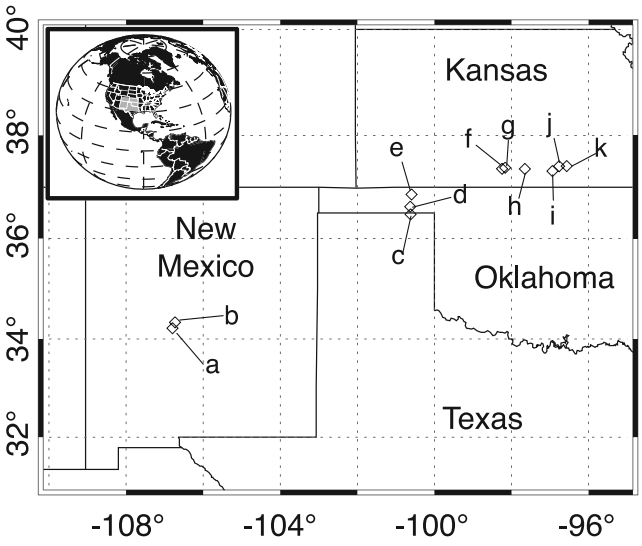

Figure 2. Map of site locations. Site labels are given in Table 1.

Irannejad [1999] also showed that selection of SHPs was far more important than the SHP model used. Additional precedent is set for this type of modification in studies such as the ones by *Morel-Seytoux et al.* [1996] and *Gutmann and Small* [2005] and by models such as UNSAT-H [*Fayer*, 2000] that allow the user to select the SHP model they prefer at runtime. In addition, we ran the Noah LSM with optimized SHPs for both the van Genuchten and the Campbell version, and found that the two versions of the model showed nearly identical results.

2.4. Site Parameters, Boundary, and Initial Conditions

[16] Weather forcing data for the models were collected from the Sevilleta National Wildlife Refuge (NWR) and Long Term Ecological Research (LTER) station grass and shrub sites of *Kurc and Small* [2004] and at nine additional sites by the International H_2O Project (IHOP) [*Weckwerth et al.*, 2004]. These 11 sites are spread out from eastern Kansas to central New Mexico, and mean annual precipitation varies from 250 to 900 mm (Figure 2 and Table 1). The following atmospheric forcing data were collected at all sites: air temperature, pressure and humidity, wind speed, and shortwave and longwave downward radiation. In addition, latent and sensible heat fluxes were measured by the Bowen Ratio method (Sevilleta grass and shrub sites), and by the eddy covariance method (IHOP sites). Table 1 summarizes the model parameters used for each site.

[17] The Sevilleta grass site is dominated by black grama (*Bouteloua eriopoda*) with 50% vegetation cover, though the fraction that is active varies over time with a typical value of 25% [*Matsui et al.*, 2003]. The Sevilleta shrub site is dominated by creosote bush (*Larrea tridentata*) and has 30% vegetation cover, most of which is active. On average, these sites get 250 mm of rain per year. Data were collected at a reference height of 2 m. Surface roughness (0.03 m grass, 0.08 m shrub) was determined as one tenth the height of vegetation cover. Albedo (0.14 grass, 0.16 shrub) was determined from measurements of incoming and outgoing radiation [*Small and Kurc*, 2003]. The soil at both sites is classified as a sandy loam.

[18] For the Sevilleta we initialized the model soil moisture as dry, consistent with observations at this site [*Small and Kurc*, 2003], and started the model 1 January the year prior to the period of interest (18 month spin-up) using continuous weather observations. To determine the model sensitivity to SHPs, we analyzed midday (12:00 to 3:00 PM) model output following a large rain storm, 33 mm at the shrub site and 10 mm at the grass site.

[19] The nine IHOP sites cover a range of annual precipitation levels and vegetation characteristics (Table 1). Mean annual precipitation ranges from 530 mm at station 1 to 900 mm at station 9. Vegetation ranges from essentially bare ground at station 1 to 80% natural grass at site 9 and with the most common species being big bluestem (*Andropogon gerardii vitman*), little bluestem (*Schizachyrium scoparium*), sand sagebrush (Artemesia filifolia), smooth sumac (*Rhus glabra*), field bindweed (*Convolvulus arvensis*), witchgrass (*Panicum capillare*), common wheat (*Triticum aestivum*), and Indian grass (*Sorghastrum nutans*). The top 2 cm soil layer included the following soil texture classes: sandy clay loam (sites 1 and 2), sandy loam (site 3), loam (site 4), clay loam (sites 5 and 6), silty clay loam (sites 7–9). The next soil layer down was usually the same texture class, at some sites silty clay and clay were also present at greater depth. Bulk densities ranged from 1.03 to 1.70 g/cm^3, and saturated moisture contents ranged from 0.32 to 0.69 (cm^3/cm^3).

[20] For these sites, we also initialized the model soil moisture dry and started the model 1 January the year prior to the period of interest (17 month spin-up). Weather forcing data were only available for 2 months, so we used HRLDAS (High-Resolution Land Data Assimilation System)

Table 1. Site Parameters[a]

Variable	SevS	SevG	IHOP 1	IHOP 2	IHOP 3	IHOP 4	IHOP 5	IHOP 6	IHOP 7	IHOP 8	IHOP 9
Map ID	a	b	c	d	e	f	g	h	i	j	k
Dominant vegetation	creosote	grass	bare	grass	sagebrush	grass	wheat	wheat	grass	grass	grass
Vegetation cover, %	30	25	5	30	45	30	50	50	70	75	80
Texture class	Sa, L	Sa, L	Sa, C, L	Sa, C, L	Sa, L	L	L	C, L	Si, C, L	Si, C, L	Si, C, L
Rain event, mm	33	10	14	17	19	29	32	24	30	96	61
MAP, mm	250	250	530	540	560	740	750	800	900	880	900
Albedo	0.16	0.14	0.25	0.21	0.18	0.21	0.19	0.20	0.23	0.25	0.19
Z_o, m	0.08	0.03	0.0024	0.024	0.029	0.011	0.059	0.049	0.023	0.018	0.012
Latitude	34.335	34.358	36.472	36.622	36.861	37.358	37.378	37.355	37.313	37.407	37.410
Longitude	−106.729	−106.701	−100.618	−100.627	−100.594	−98.245	−98.164	−97.653	−96.939	−96.766	−96.567

[a]Texture classes are as follows: Sa, sand; L, loam; Si, silt; C, clay. MAP is mean annual precipitation. Z_o is surface roughness.

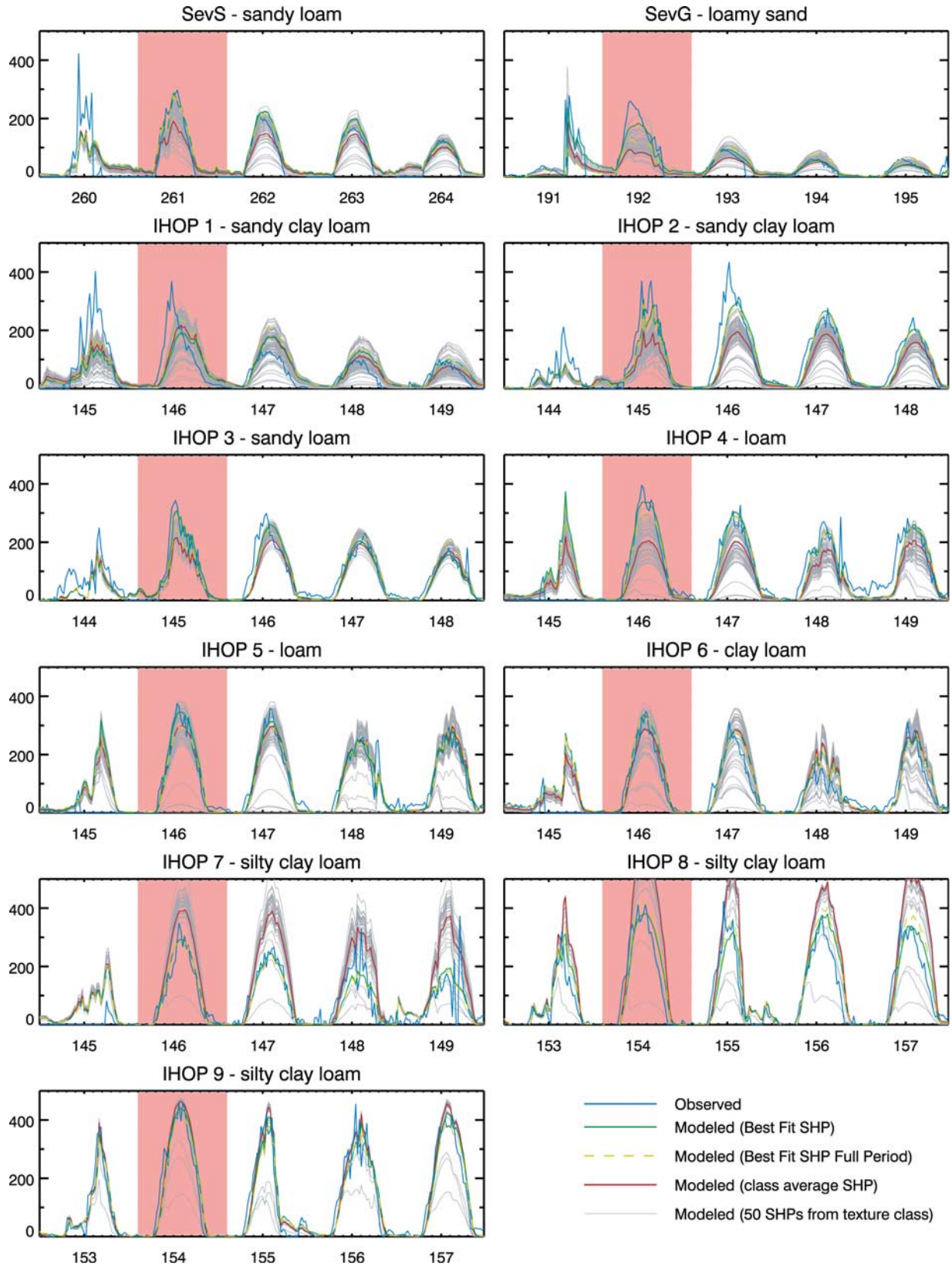

Figure 3. Time series of latent heat flux following a rainstorm at each site. Statistics for Tables 2a and 2b come from the day with shaded background. The X axis is the day of the year. A random subset of 50 soil hydraulic properties (SHPs) (dotted line) is presented at each site because if all soils are shown, it becomes impossible to distinguish individual lines. Individual SHPs (gray dotted line) come from the real soil texture class at each site. Measured LH (blue line), best fit SHP LH (green line), best fit SHP for the entire period LH (yellow dashed line), and texture class average SHP LH (red line) are also shown.

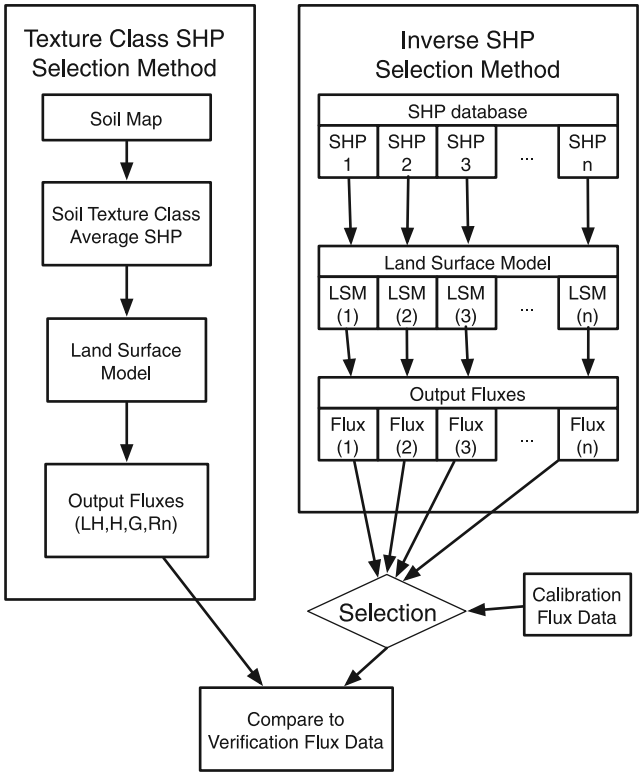

Figure 4. Flowchart for soil hydraulic property (SHP) selection procedures. Commonly, researchers use a soil texture class (shown on the left) to determine SHPs. Inverse methods (shown on the right) use a measure of model performance to determine model parameters. We then compare both methods' prediction of LH to measured LH.

[*Chen et al.*, 2004] data to spin up the model. These data are not ideal because they are not local measurements, but they represent the best estimate for each site. We repeated all of the analyses with a spin-up period developed by looping over the available weather data, and found it had little to no effect on the results.

[21] For most IHOP sites, the closure of the energy balance from measured fluxes (equation (5)) generally ranged from 0.8 to 1.2.

$$closure = \frac{LH + H}{R_n - G} \tag{5}$$

where LH is latent heat flux, H is sensible heat flux, R_n is net radiation, and G is ground heat flux. Periods in which closure was below 0.8 were excluded from the analysis. Closure was never above 1.2 for a significant period. For sites 7 and 8, closure was often as low as 0.4. This error is likely to come from the measurement of LH and sensible heat flux (H) [*Twine et al.*, 2000]. To correct errors in closure, we adjusted the measured LH to force closure while keeping the bowen ratio constant (equation (6)).

$$LH^* = LH + \frac{1}{2} LH \frac{\overline{R_n} - \overline{G}}{\overline{\lambda E} + \overline{H}} \tag{6}$$

where LH^* is the corrected latent heat flux, and $\overline{X}$ denotes the mean value of X for the day of the current measurement. Closure was forced on a daily basis, not for individual measurements. While this will not remove all of the error in the flux measurements, it makes them consistent with the radiation measurements which are supplied to the model as inputs. Sevilleta flux measurements were made by the Bowen Ratio method and inherently have a closure of 1.

2.5. Model Experiments

[22] We selected a single rain event for part of these experiments because the short IHOP record did not include multiple complete dry down events at all sites. The rain event used for these experiments was selected based on the measured flux data. First, midday energy balance closure (equation (5)) for measured data on the days following the event was required to be between 0.8 and 1.2 following the storm. Then the storm with the largest measured LH response was selected. Measured LH for the selected interval is shown for all sites in Figure 3. For seven of the nine IHOP sites we used the same storm. IHOP 8 and 9 had poor energy balance closure during this storm, so a later storm was used at those sites. The size of the event varied from site to site (Table 1).

2.5.1. Soil Texture Class as a Predictor

[23] The following modeling experiment was designed to test the effectiveness of texture class average SHPs. We assume that the SHPs in the database of *Schaap and Leij* [1998] represent the real distribution of SHPs within each texture class, and we treat LH output from model runs with these SHPs as the expected distribution of fluxes. We then examine how well model runs with soil texture class average SHPs predict this expected distribution of LH fluxes.

[24] We ran the Noah model once for each soil in the SHP database of *Schaap and Leij* [1998], and for the texture class average SHPs. The complete spin-up period was run separately for each set of SHPs. We compared these model runs by their midday (12:00 to 3:00 PM) average latent heat flux (LH) on the day after a rain event. We calculated how well a model using texture class average SHPs predicts the model output from the distribution of SHPs in the database via equation (7). Equation (7) computes the coefficient of determination for the relationship as 1 minus the ratio of the sum of the squared model residuals to the sum of the square deviations from the mean. This step was performed independently for each site.

$$r^2 = 1 - \frac{\sum_{i=0}^{n} \left(LH(SHP_i) - LH(SHP_{STC})\right)^2}{\sum_{i=0}^{n} \left(LH(SHP_i) - \overline{LH(SHP_i)}\right)^2} \tag{7}$$

where r^2 is the predictive capability of soil texture class at a site (similar to the Nash-Sutcliffe efficiency). $LH(SHP_i)$ is the LH from a model run at a site with the SHP of the ith soil. $LH(SHP_{STC})$ is the LH from a model run with the SHP of the soil texture class average for the texture of the ith soil. $\overline{LH(SHP_i)}$ is the mean LH at a site from all model runs.

[25] To remove the bias in the database toward coarser texture soils, a random subset of 50 soils was selected from each texture class. r^2 was calculated independently for 100 random subsets and the average of those 100 subsets was used. For the silt clay loam, sandy clay, and silty clay

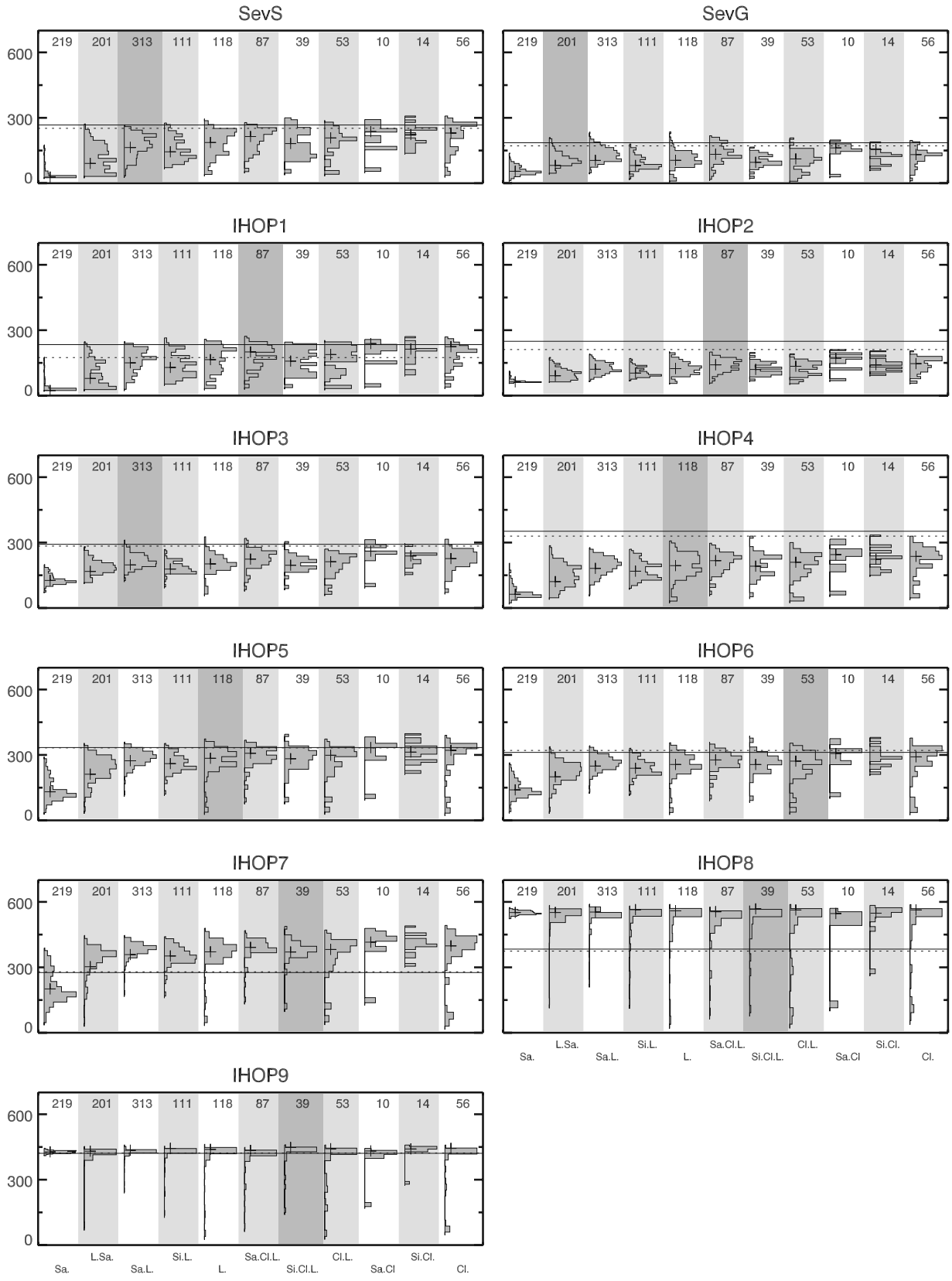

Figure 5. Histograms of midday latent heat flux resulting from the variability of SHPs within each soil texture class on the day after a rainstorm. Best fit LH (dotted line), measured LH (solid line), and class average LH (crosses) are plotted on top of the histograms. The actual texture class for each site is shaded in dark grey. Histograms are normalized as in Figure 1.

Table 2a. Average Range of Modeled LH Within and Between Soil Texture Classes

Predictor	SevS	SevG	IHOP 1	IHOP 2	IHOP 3	IHOP 4	IHOP 5	IHOP 6	IHOP 7	IHOP 8	IHOP 9
Average LH range within texture classes, W/m^2	242	182	180	134	212	250	297	278	362	483	339
LH range of texture class medians, W/m^2	129	87	119	73	84	104	97	92	78	19	18

texture classes all available soils were used because the database contained fewer than 50 soils in these texture classes.

2.5.2. Inverse Modeling

[26] We analyze the degree to which model output can be improved by careful SHP selection by comparing measured LH to modeled LH with SHPs selected by an inverse procedure. The inverse procedure we used to select the best SHP for each site (Figure 4) was designed to minimize error between measured and modeled LH. To select the best SHP, we ran the Noah model for all SHPs in the database, and selected the SHP used in the model run that provided the best fit to the measured data. This simplified the search domain to 1306 SHP combinations, and forced the SHPs to be realistic combination of parameters. Other inverse methodologies [e.g., *Gupta et al.*, 1998; *Bastidas et al.*, 1999; *Vrugt et al.*, 2003] are also appropriate.

[27] For this experiment, we selected the best SHPs at each site for a single dry down event, and for the entire period for which good LH measurements were available. The dry down events were selected based on the criteria used in the previous section. A four to six day window of clear days following the rain event were used for the inverse procedure, and a single day following the event was used for comparison. We used up to six days because this was identified by *Kurc and Small* [2004] as being the most important period for dry down dynamics. When fitting the entire record we used any days in which closure was within 0.15 of 1.0 and midday LH was greater than 50. For the IHOP sites, we only used days that were after the first 10 days of measured data to allow the model to adjust to any possible discrepancies between the HRLDAS forcing and the measured weather forcing. We were unable to perform a calibration on one rain storm and a comparison based on another due to the brevity of the IHOP records. However, by fitting the full LH record we have an independent estimate to be used for verification. For comparisons between sites, we removed the site to site variability in potential evaporation by looking at the evaporative fraction (EF equation (8)).

$$EF = \frac{LH}{R_n - G} \tag{8}$$

where R_n is net radiation, and G is ground heat flux. We then compared the measured LH to the model output using the inverse SHP from a single dry down, the inverse SHP from the full period, and the texture class average SHP. We use this comparison to quantify how well it is possible to improve the model output by modifying SHPs.

[28] To confirm that the SHPs selected with this methodology are optimal for a site not just for a single storm, "best" SHPs were selected for a series of different storms at the Sevilleta shrub site, which has a multiyear record. We selected all rain storms greater than 5 mm, and then used the measured LH on the following six days to optimize SHPs for each storm. If another rainstorm greater than 2 mm occurred after the first two days, then only the days prior to that storm were used for calibration. If another storm greater than 2 mm occurred within 2 days of the large storm than no SHPs were selected [*Kurc and Small*, 2004]. If rain continued for several days in a row, then the storm size was calculated including rain fall over the two days prior to the main rain event. Additionally, only days for which the midday measured LH was greater than 100 W/m^2 were used. These criteria led to the selection of 7 storms. The resulting SHPs from all 7 storms were compared in addition to the SHPs for various soil texture classes. Storm sizes used were, 23, 17, 12, 9, 10, 33, and 11 mm, in chronological order.

2.5.3. Vegetation Effects

[29] To examine the effect of vegetation, we looked at the variability in model output caused by SHPs as vegetation cover was varied. We present results from IHOP site 8, though other sites show a similar pattern. We ran all soils in the database and varied vegetation cover from 0 to 100% in 10% increments. We then compared the mean LH and the 10th and 90th LH percentiles at each vegetation level on the day after a 25 mm rainstorm. This is not the same storm used in the previous sections because we did not require LH measurements for this analysis, and the storm used in the previous section was substantially larger than normal.

3. Results and Discussion

[30] For all texture classes, at most sites, modeled latent heat flux (LH) is low (0–150 W/m^2) before a rain storm, and higher (100–600 W/m^2) after (Figure 3). Measured LH follows a similar pattern across all sites, low (50–200 W/m^2) before and higher (250–450 W/m^2) after the storm. In all cases the texture class average model LH falls near the middle of the distribution of modeled LH, however, the measured LH sometimes falls near the middle (IHOP 1, 5, 6, 9), the bottom (IHOP 7, 8) or the top (SevS, SevG, IHOP 2, 3, 4) of the distribution. In some cases, the measured LH starts at the high end of the model distribution, and decreases to the low end of the distribution over the course of the dry down (SevS, SevG, IHOP 1, 3). Differences between the measured LH and the model LH distribution may be due to variations in SHPs from site to site, model structure error, errors in other model parameters, or simply to errors in the measurement of either the meteorological forcing or the resultant fluxes. To examine the effect of SHP variability within the database we look at the distribution of LH on the day following the storm.

3.1. Soil Texture Class as a Predictor

[31] On the day following the storm, LH values varied more within a soil texture class than they do between soil texture classes at all sites (Figure 5). In general, midday LH varies by 200–300 W/m^2 within a soil texture class, but the median values from each class only vary by 100 W/m^2

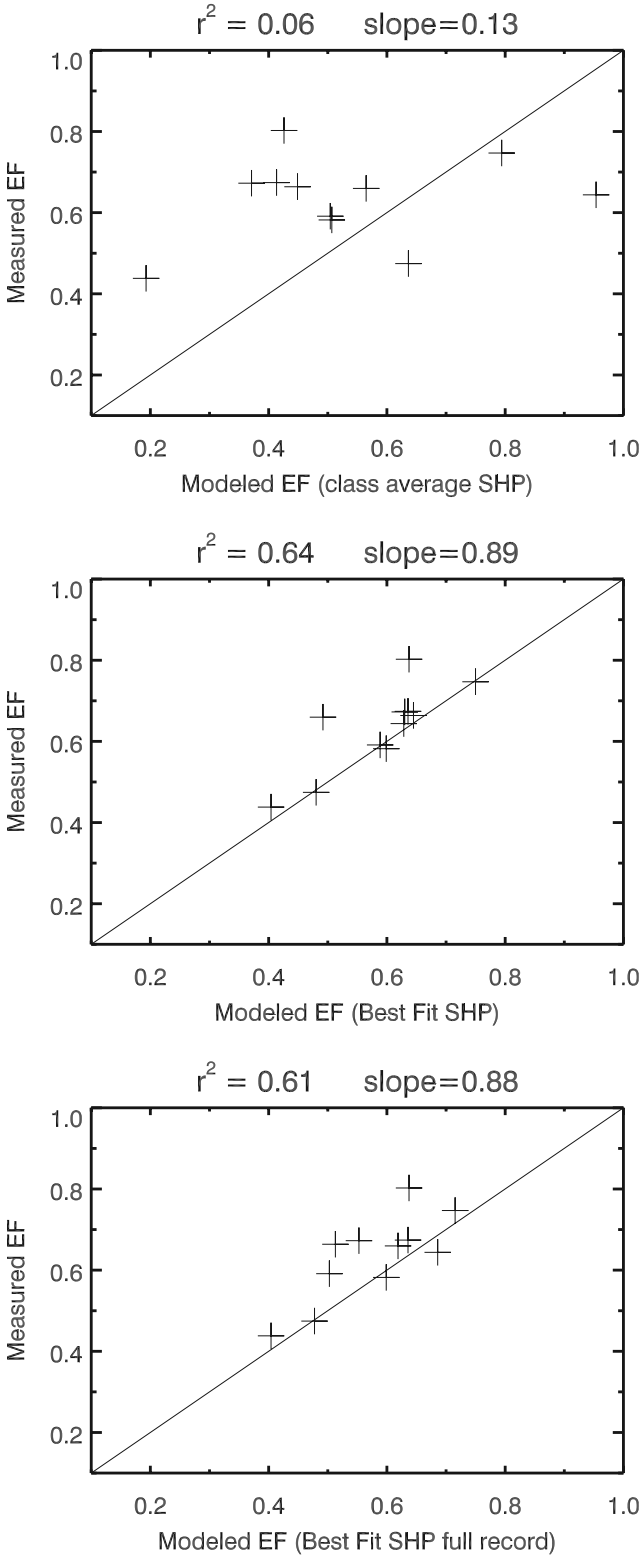

Figure 6. (top) Soil texture class average evaporative fraction (EF = LH/(Rn − G)) versus measured EF, (middle) best fit EF versus measured EF, and (bottom) best fit full record EF versus measured EF. One to one line is drawn for reference, and the slope and correlation of the regression line are above each graph.

(Table 2a). This indicates that soil texture class represents a small percentage of the total variation in LSM fluxes that is due to SHPs. The exceptions to this distribution are the sand texture class, and IHOP sites 8 and 9, in which there is much less variation in model LH. These exceptions will be discussed at the end of this section. In addition, for 5 of the 11 sites, the measured LH falls near the top of the model LH distribution. The texture class average model LH often falls in the middle of the model LH distribution, and in several cases, it falls below the mode of the distribution. This might indicate a bias in the texture class average values.

[32] To quantify how well soil texture class works as a predictor, we calculate coefficients of determination (r^2) between model LH and several predictor variables: texture class (equation (7)), particle size distributions (texture), van Genuchten m, and log(Ks). These relationships are often nonlinear, so we used a fourth-order polynomial in the regression for all variables other than texture class average. Because of the nature of the sand class, we treat it as an outlier and do not include it in these calculations. The van Genuchten m parameter explains the vast majority of variance in modeled LH output (46–72%, Table 2b) at sites with less vegetation cover. At sites with more vegetation cover (greater than 50%), Ks explains most of the variance in model LH (46–76%). In contrast, soil texture class explains 0–15% of the variance in modeled LH. It is possible to improve on soil texture class by using the particle size distributions (percent sand, silt, and clay). However, even with this additional information, it is only possible to explain 8–24% of the variance in LH.

[33] The limited utility of soil texture is expected given the imperfections of pedotransfer functions, as demonstrated by *Soet and Stricker* [2003]. Our study may be a slight over estimate of the range of output values because the SHPs used are based on small soil samples which may show more variability than site-scale SHPs. However, it is unlikely that using SHPs derived at an appropriate scale would substantially improve the correlation with texture class, and in

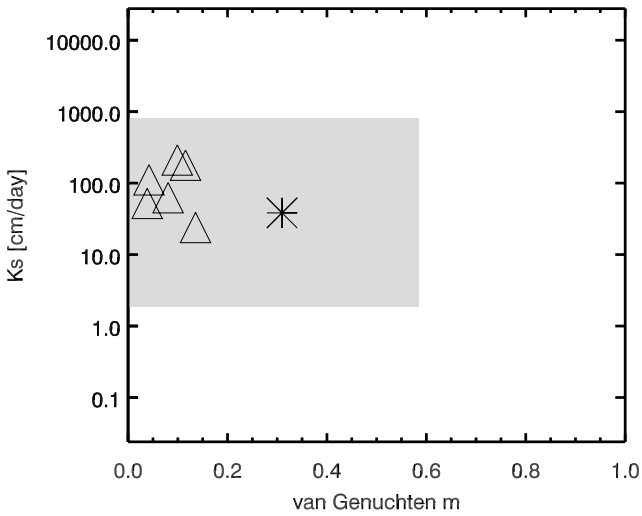

Figure 7. SHPs selected from multiple storms for the Sevilleta shrub site (triangles). Sandy loam soil texture class average SHPs (asterisk) is shown with $\pm 2\sigma$ in gray. X and Y axis ranges were set to the minimum and maximum values in the SHP database.

Table 2b. Summary of r^2 Values Between Measured and Modeled Evaporative Fraction Using Different SHP and Texture Predictor Variables in a Fourth-Order Polynomial (K_s, m, and Sand, Silt, Clay) or Texture Class Average Model Output as a Predictor Variable (Equation 7)[a]

Predictor	SevS	SevG	IHOP 1	IHOP 2	IHOP 3	IHOP 4	IHOP 5	IHOP 6	IHOP 7	IHOP 8	IHOP 9
log(K_s)	0.32	0.35	0.26	0.27	0.36	0.27	0.38	0.35	**0.46**	**0.76**	**0.65**
m	**0.72**	**0.63**	**0.72**	**0.63**	**0.46**	**0.66**	**0.48**	**0.47**	0.29	0.01	0.01
Texture class	0.15	0.07	0.06	0.09	0.04	0.13	<0.01	<0.01	<0.01	<0.01	<0.01
Sand, silt, clay	0.24	0.16	0.23	0.21	0.17	0.19	0.15	0.14	0.12	0.09	0.08

[a]See text. The best r^2 is in bold for each site.

addition, other sources of variability are likely to be introduced in the effective SHPs at larger scales that are not accounted for by the SHPs in this database.

[34] The sand texture class is significantly different from all other soil texture classes (Figure 5). Within the sand class, LH only varies by 50–300 W/m^2, and at most sites, modeled LH falls within a 50 W/m^2 range. Interestingly, the sand class shows more variation at most of the sites with 50% or greater vegetation cover (IHOP 5, 6, 7). It is critical that LSMs can distinguish between more than just sand and nonsand because, in a larger soils survey of 15737 soils across the United States, sands constitute only 5% of soils [*Carsel and Parrish*, 1988].

[35] IHOP sites 8 and 9 show a different pattern from the other sites (Figure 5). At these two sites, the majority of modeled LH values fall in a very narrow range. This may be due to a combination of two factors. Both of these sites have a very large rainfall event (96 and 61 mm respectively), and both of these sites have more vegetation cover (75% and 80%) than the other sites. While there are SHPs at site 8 that fit the measured LH, they are outside of the normal range. It is likely that the measured LH at this site does not fit the typical distribution of model LH, due to model structure error. This will be discussed further in the inverse modeling section below.

3.2. Inverse Modeling

[36] Inverse selection of SHPs reduce RMS errors between measured and modeled midday LH from 88 W/m^2 to 28 W/m^2 for SHPs fit to the individual storm and to 39 W/m^2 for SHPs fit to the entire record. Inverse methods increased the correlation between measured and modeled EF in this study from $r^2 = 0.06$ to $r^2 = 0.64$ and $r^2 = 0.61$ respectively (Figure 6). The slope between predicted and modeled EF changes from 0.13 to 0.89 and 0.88 respectively. Because EF includes net radiation and ground heat flux, and we have selected data with reasonable energy balance closure, this shows that SH is also fit better as the sensible heat fraction equals one minus EF. This clearly illustrates that when texture class is used to predict SHPs, very little of the site to site variability is accurately predicted by the model, and the variability that is predicted may be a function of other parameters such as vegetation cover and storm size. Additionally, though results are comparable when SHPs are fit to the dry down in question or to the full period, RMS errors are improved when the model is fit to the individual dry down. These results are not limited to sparsely vegetated areas, though the expected distribution of model LH (Figure 3) suggests that SHPs are more important in areas with less vegetation cover.

[37] Inversely derived SHPs are effective calibration parameters for the entire soil column. Ideally SHPs would be derived for each major soil horizon, but the inverse problem is likely to be ill posed when the number of parameters increases substantially. In addition, LSMs are often used with vertically constant SHPs. As a result, it is better to derive effective SHPs for the entire column.

[38] It is clear that our inverse selection of SHPs produces consistent results. When the inverse procedure was applied independently to multiple storms at the Sevilleta shrub site, SHPs generated for each storm were similar. The differences between SHPs generated for different storms were small relative to the difference between them and the texture class average SHP (Figure 7). In both the Ks and m parameters, the two most important parameters as shown in Table 2b, the variation in best fit parameters between storms was also much less than the variation within the texture class as a whole. Ks values fell between $10^{1.5}$ and $10^{2.5}$, while sandy loams typically range from $10^{0.2}$ to 10^3. m values ranged from 0.05 to 0.15, while sandy loams typically range from 0 to 0.55.

[39] Inverse methods clearly produce LSM parameter sets that more accurately reflect measured LH and SH values, but these parameter sets may be compensating for errors in other LSM parameters, errors in model structure, or errors in the input or measured data sets. The most likely examples of this in our data set are IHOP sites 2 and 8. At these sites the measured LH values fall significantly outside the typical distribution of LH values. Both of these sites had a very large rain event with site 8 having more vegetation cover and site 1 being almost bare ground. It is likely that these differences between model and measured LH are due

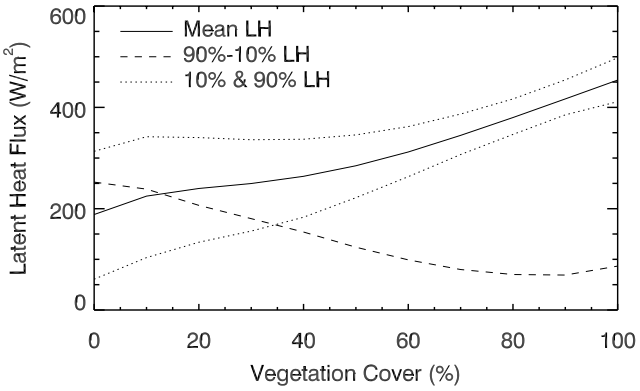

Figure 8. Effects of increasing vegetation cover. Mean LH (solid line), 10th and 90th percentiles (dotted lines), and the range from the 90th to the 10th percentile (dashed line) for the distribution of SHPs are plotted for IHOP 8.

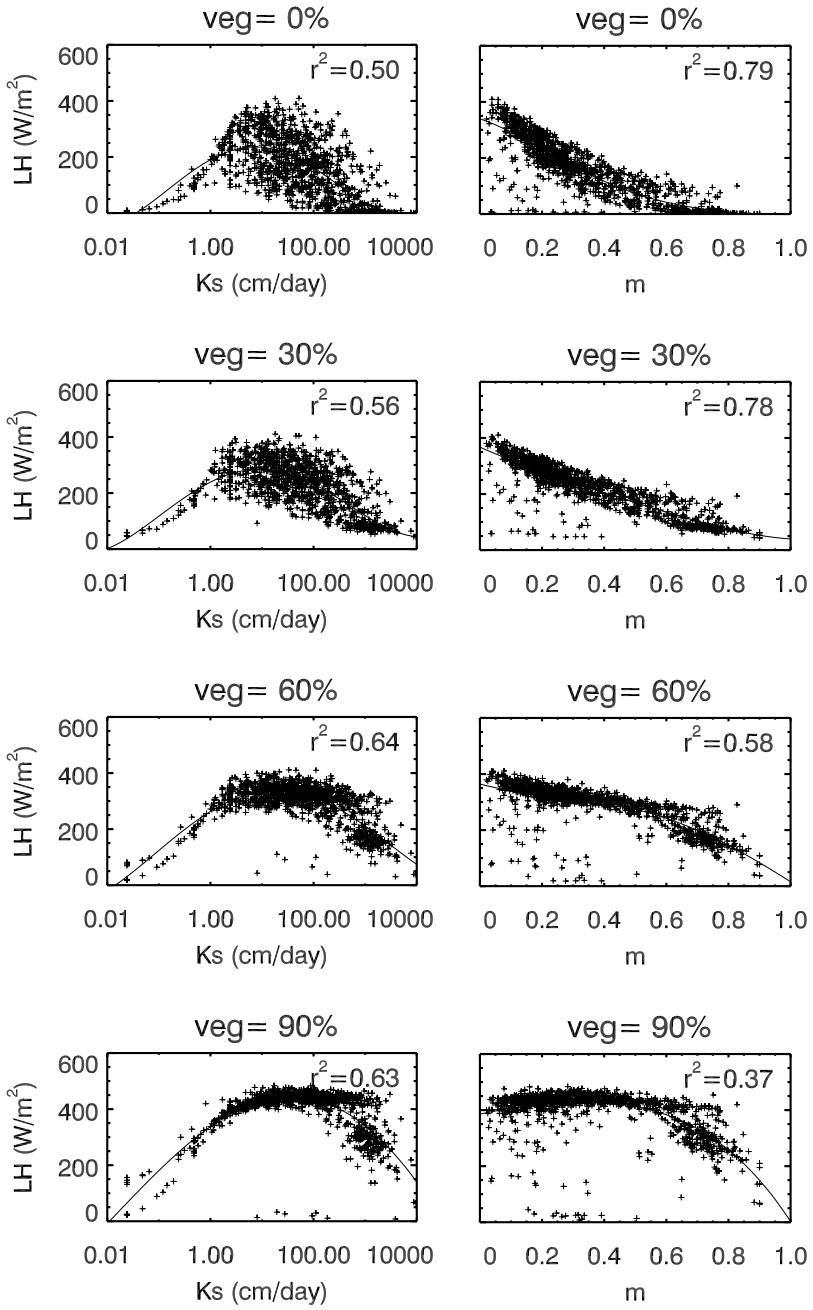

Figure 9. Effects of increasing vegetation cover on the relative importance of (left) Ks and (right) m. As vegetation increases from 0 to 90% cover (from top to bottom), the distribution of model LH is more sensitive to Ks and less sensitive to m. The majority of soils in the cluster of high Ks, high m, and low LH are in the sand class.

to a combination of model structure error and LH measurement error. Because an inverse procedure incorporates these other sources of error, it may be necessary to use inversely derived SHPs within the same modeling framework that they are derived in. The transferability of SHPs between sites and models is the subject of other research studies [e.g., *Hogue et al.*, 2005] and should be studied more in the future.

3.3. Vegetation Effects

[40] Increasing vegetation cover changes the impact of SHPs on Noah model output. The average LH response increases from 190 to 450 W/m^2 as model vegetation cover increases from 0 to 100% at IHOP site 8 (Figure 8). In contrast, the difference between the 10th and 90th percentile of LH decreases from 150 to 30W/m^2, with a corresponding decrease in the coefficient of variation from 0.5 to 0.16. This is likely to occur because vegetation is able to draw water from the top 3–4 model soil layers, depending on the rooting depth. Thus LH is less affected by movement of water from one layer to the next for vegetated areas than for bare soil. Because this movement is strongly controlled by SHPs, SHPs have less effect on the Noah LSM when substantial vegetation cover is present. However, drainage

below the root zone, the distribution of water within the root zone, and surface runoff are controlled by SHPs as well and these effect LH even with more vegetation cover. With increased vegetation cover, texture class still does not predict the variation caused by SHPs, but that variation is a smaller percent of the total LH.

[41] In addition, the variation in LH within the sand class actually increases with increasing vegetation cover. This result is not seen in the model runs shown in Figure 5 because the storms used in Figure 5 for IHOP sites 8 and 9 are dramatically larger (96 and 61 mm). At that point the soil was completely saturated for almost all SHPs. It was not possible to use the smaller storm for the earlier section of this study because there were problems with the LH measurements during that period.

[42] The importance of different SHP parameters changes as vegetation cover increases (Figure 9). As vegetation cover increases, the amount of variability in LH explained by the m parameter changed from 79 to 37%, while the variability explained by Ks increases from 50 to 63%. Note that the sum of these r^2 values is greater than one due to correlation between Ks and m. This occurs because, as vegetation cover increases, the source of variability shifts from water movement between the topsoil layers to variations in runoff and deep infiltration. Runoff and deep infiltration are primarily controlled by Ks rather than m and thus Ks becomes a more important parameter.

4. Conclusions

[43] The use of soil texture class alone is not an adequate method of determining SHPs for LSMs. The main functions of LSMs in climate and weather modeling is the calculation of energy and moisture fluxes to the atmosphere. Of the total variance in these fluxes, soil texture class accounts for only 5%, while the van Genuchten m and saturated conductivity parameters explain 56 and 62% respectively. Additionally, we have shown that it is possible to explain 20% of the variance if particle size fractions are used to predict LH, but if a pedotransfer function is used to predict SHPs from particle size fractions, the additional intermediate step is likely to decrease this value. These results are generally consistent for all surface fluxes in the Noah model, with and without vegetation cover, over a range of climatic regimes, and indicate the importance of properly estimating SHPs.

[44] Because of the inherent difficulties of measuring SHPs directly, especially on a global scale, we suggest that this data set must be constructed via inverse modeling based upon remotely sensed data sources such as skin temperature derived from IR measurements or soil moisture derived from microwave systems [e.g., *Burke et al.*, 1998] or from the Gravity Recovery and Climate Experiment (GRACE). The work of *Burke et al.* [1998] showed a derivation of SHPs from a passive microwave system, but more work needs to be done to determine how well SHPs can be derived globally from remotely sensed data sets. We have shown that inverse methods reduced RMS errors in the Noah model LH from 88 to 28 W/m^2, and that the SHPs derived through inverse modeling are consistent across different periods of a longer record. Inverse methods are a better method of deriving SHPs for LSMs because of issues related to scale and model structure. Inverse methods derive SHPs at a scale commensurate with LSMs, as compared to conventional methods which measure SHPs over a small ($\approx$100 cm^2) area. SHPs derived from inverse modeling incorporate errors in model structure, and non-SHP parameters. As a result, inversely derived SHPs must be used within the same model as they are derived in, with the same non-SHP parameters.

[45] Finally, we have shown that the importance of SHPs with respect to LH decreases with increasing vegetation cover, and that the dominant SHP changes from the van Genuchten m parameter to the saturated conductivity. The mean LH value increases with increasing vegetation cover, but the coefficient of variation of LH between SHPs decreased by from 0.50 to 0.16. This change occurs because of decreasing importance of soil water movement when vegetation is able to draw water from a range of depths.

[46] **Acknowledgments.** This research was partially supported by NNG04GO83G (CU Boulder) from the NASA Earth Science Enterprise (program manager J. Entin). The field data used to run the model were collected via partial support by SAHRA (Sustainability of semi-Arid Hydrology and Riparian areas) under the STC Program of the National Science Foundation, Agreement No. 9876800. Logistical support was provided by the Sevilleta LTER Program (NSF Grant DEB-0080529).

References

Arya, L., F. Leij, M. van Genuchten, and P. Shouse (1999), Scaling parameter to predict the soil water characteristic from particle-size distribution data, *Soil Sci. Soc. Am. J.*, *63*, 510–519.

Bastidas, L., H. Gupta, S. Sorooshian, W. Shuttleworth, and Z. Yang (1999), Sensitivity analysis of a land surface scheme using multicriteria methods, *J. Geophys. Res.*, *104*, 19,481–19,490.

Bonan, G., S. Levis, S. Sitch, M. Vertenstein, and K. Oleson (2003), A dynamic global vegetation model for use with climate models: Concepts and description of simulated vegetation dynamics, *Global Change Biol.*, *9*, 1543–1566.

Braud, I., D. De Condappa, J. Soria, R. Haverkamp, R. Angulo-Jaramillo, S. Galle, and M. Vauclin (2005), Use of scaled forms of the infiltration equation for the estimation of unsaturated soil hydraulic properties (the Beerkan method), *Eur. J. Soil Sci.*, *56*, 361–374.

Burke, E., R. Gurney, L. Simmonds, and P. O'Neill (1998), Using a modeling approach to predict soil hydraulic properties from passive microwave measurements, *IEEE Trans. Geosci. Remote Sens.*, *36*, 454–462.

Campbell, G. (1974), Simple method for determining unsaturated conductivity from moisture retention data, *Soil Sci.*, *117*, 311–314.

Carsel, R., and R. Parrish (1988), Developing joint probability-distributions of soil-water retention characteristics, *Water Resour. Res.*, *24*, 755–769.

Chen, F., and J. Dudhia (2001), Coupling an advanced land surface-hydrology model with the Penn State-NCAR MM5 modeling system. Part I: Model implementation and sensitivity, *Mon. Weather Rev.*, *129*, 569–585.

Chen, F., K. Manning, D. Yates, M. LeMone, S. Trier, R. Cuenca, and D. Niyogi (2004), Development of high resolution land data assimilation system and its application to WRF, paper presented at AMS 16th Conference on Numerical Weather Prediction, Am. Meteorol. Soc., Seattle, Wash.

Clapp, R., and G. Hornberger (1978), Empirical equations for some hydraulic properties, *Water Resour. Res.*, *14*(4), 601–604.

Dickinson, R., A. Henderson-Sellers, and P. Kennedy (1993), Biosphere-Atmosphere Transfer Scheme (BATS) version 1e as coupled to the NCAR Community Climate Model, *NCAR Tech. Note TN-387+STR*, Natl. Cent. for Atmos. Res., Boulder, Colo.

Duan, Q., et al. (2006), Model parameter estimation experiment (MOPEX): An overview of science strategy and major results from the second and third workshops, *J. Hydrol.*, *320*, 3–17.

Ek, M., K. Mitchell, Y. Lin, E. Rogers, P. Grunmann, V. Koren, G. Gayno, and J. Tarpley (2003), Implementation of Noah land surface model advances in the national centers for environmental prediction operational mesoscale eta model, *J. Geophys. Res.*, *108*(D22), 8851, doi:10.1029/2002JD003296.

Fayer, M. (2000), UNSAT-H version 3.0: Unsaturated soil water and heat flow model theory, user manual, and examples, *Tech. Rep. PNNL-13249*, Pac. Northwest Natl. Lab., Richland, Wash.

Feddes, R., M. Menenti, P. Kabat, and W. Bastiaanssen (1993), Is large-scale inverse modeling of unsaturated flow with areal average evaporation and surface soil-moisture as estimated from remote-sensing feasible, *J. Hydrol.*, *143*, 125–152.

Gupta, H., S. Sorooshian, and P. Yapo (1998), Toward improved calibration of hydrologic models: Multiple and noncommensurable measures of information, *Water Resour. Res.*, *34*, 751–763.

Gutmann, E., and E. Small (2005), The effect of soil hydraulic properties vs. soil texture in land surface models, *Geophys. Res. Lett.*, *32*, L02402, doi:10.1029/2004GL021843.

Hoffmann-Riem, H., M. van Genuchten, and H. Fluhler (1999), A general model of the hydraulic conductivity of unsaturated soils, in *Proceedings of the International Workshop, Characterization and Measurements of the Hydraulic Properties of Unsaturated Porous Media*, edited by M. van Genuchten, F. Leij, and L. Wu, pp. 31–42, Univ. of Calif., Riverside.

Hogue, T., L. Bastidas, H. Gupta, S. Sorooshian, K. Mitchell, and W. Emmerich (2005), Evaluation and transferability of the Noah land surface model in semiarid environments, *J. Hydrometeorol.*, *6*, 68–84.

Kabat, P., R. Hutjes, and R. Feddes (1997), The scaling characteristics of soil parameters: From plot scale heterogeneity to subgrid parameterization, *J. Hydrol.*, *190*, 363–396.

Kravchenko, A., and R. Zhang (1998), Estimating the soil water retention from particle-size distributions: A fractal approach, *Soil Sci.*, *163*, 171–179.

Kurc, S., and E. Small (2004), Dynamics of evapotranspiration in semiarid grassland and shrubland ecosystems during the summer monsoon season, central New Mexico, *Water Resour. Res.*, *40*, W09305, doi:10.1029/2004WR003068.

Leij, F., W. Alves, M. van Genuchten, and J. Williams (1996), Unsaturated soil hydraulic database, UNSODA 1.0 user's manual, *Rep. EPA/600/R96/095*, U.S. Environ. Prot. Agency, Ada, Okla.

Leij, F., W. Russell, and S. Lesch (1997), Closed-form expressions for water retention and conductivity data, *Ground Water*, *35*, 848–858.

Liang, X., and J. Guo (2003), Intercomparison of land-surface parameterization schemes: Sensitivity of surface energy and water fluxes to model parameters, *J. Hydrol.*, *279*, 182–209.

Liang, X., Z. Xie, and M. Huang (2003), A new parameterization for surface and groundwater interactions and its impact on water budgets with the variable infiltration capacity (VIC) land surface model, *J. Geophys. Res.*, *108*(D16), 8613, doi:10.1029/2002JD003090.

Mahrt, L., and M. Ek (1984), The influence of atmospheric stability on potential evaporation, *J. Clim. Appl. Meteorol.*, *23*, 222–234.

Manabe, S. (1969), Climate and ocean circulation: 1. The atmospheric circulation and the hydrology of the Earth's surface, *Mon. Weather Rev.*, *97*, 739–805.

Matsui, T., V. Lakshmi, and E. Small (2003), Links between snow cover, surface skin temperature, and rainfall variability in the North Am. monsoon system, *J. Clim.*, *16*, 1821–1829.

Maxwell, R., and N. Miller (2005), Development of a coupled land surface and groundwater model, *J. Hydrometeorol.*, *6*, 233–247.

Milly, P. (1987), Estimation of Brooks-Corey parameters from water-retention data, *Water Resour. Res.*, *23*, 1085–1089.

Morel-Seytoux, H., P. Meyer, M. Nachabe, J. Touma, M. van Genuchten, and R. Lenhard (1996), Parameter equivalence for the Brooks-Corey and van Genuchten soil characteristics: Preserving the effective capillary drive, *Water Resour. Res.*, *32*, 1251–1258.

Pitman, A. (2003), The evolution of, and revolution in, land surface schemes designed for climate models, *Int. J. Climatol.*, *23*, 479–510.

Poulsen, T., P. Moldrup, T. Yamaguchi, and O. Jacobsen (2000), Predicting saturated and unsaturated hydraulic conductivity in undisturbed soils from soil water characteristics, *Soil Sci.*, *164*, 877–887.

Schaap, M., and F. Leij (1998), Database-related accuracy and uncertainty of pedotransfer functions, *Soil Sci.*, *163*, 765–779.

Schaap, M., F. Leij, and M. van Genuchten (2001), Rosetta: A computer program for estimating soil hydraulic parameters with hierarchical pedotransfer functions, *J. Hydrol.*, *251*, 163–176.

Sellers, P. J., Y. Mintz, Y. C. Sud, and A. Dalcher (1986), A simple biosphere model (SiB) for use within general circulation models, *J. Atmos. Sci.*, *43*, 505–531.

Sellers, P., S. Los, C. Tucker, C. Justice, D. Dazlich, G. Collatz, and D. Randall (1996), A revised land surface parameterization (SiB2) for atmospheric GCMs part II: The generation of global fields of terrestrial biophysical parameters from satellite data, *J. Clim.*, *9*, 706–737.

Shao, Y., and P. Irannejad (1999), On the choice of soil hydraulic models in land surface schemes, *Boundary Layer Meteorol.*, *90*, 83–115.

Small, E., and S. Kurc (2003), Tight coupling between soil moisture and the surface radiation budget in semiarid environments: Implications for land-atmosphere interactions, *Water Resour. Res.*, *39*(10), 1278, doi:10.1029/2002WR001297.

Soet, M., and J. Stricker (2003), Functional behaviour of pedotransfer functions in soil water flow simulation, *Hydrol. Processes*, *17*, 1659–1670.

Sridhar, V., R. Elliott, and F. Chen (2003), Scaling effects on modeled surface energy-balance components using the Noah-OSU land surface model, *J. Hydrol.*, *280*, 105–123.

Stolte, J., J. Freijer, W. Bouten, C. Dirksen, J. Halbertsma, J. Vandam, J. Vandenberg, G. Veerman, and J. Wosten (1994), Comparison of 6 methods to determine unsaturated soil hydraulic conductivity, *Soil Sci. Soc. Am. J.*, *58*, 1596–1603.

Twine, T., W. Kustas, J. Norman, D. Cook, P. Houser, T. Meyers, J. Prueger, P. Starks, and M. Wesely (2000), Correcting eddy-covariance flux underestimates over a grassland, *Agric. For. Meteorol.*, *103*, 279–300.

van Genuchten, M. (1980), A closed-form equation for prediction of the hydraulic properties of unsaturated soils, *Soil Sci. Soc. Am. J.*, *44*, 892–898.

Vrugt, J., H. Gupta, L. Bastidas, W. Bouten, and S. Sorooshian (2003), Effective and efficient algorithm for multiobjective optimization of hydrologic models, *Water Resour. Res.*, *39*(8), 1214, doi:10.1029/2002WR001746.

Weckwerth, T., et al. (2004), An overview of the international H_2O project (IHOP 2002) and some preliminary highlights, *Bull. Am. Meteorol. Soc.*, *85*, 253–277.

Wosten, J., Y. Pachepsky, and W. Rawls (2001), Pedotransfer functions: Bridging the gap between available basic soil data and missing soil hydraulic characteristics, *J. Hydrol.*, *251*, 123–150.

Yeh, P., and E. Eltahir (2005), Representation of water table dynamics in a land surface scheme. Part I: Model development, *J. Clim.*, *18*, 1861–1880.

Zhu, J., and B. Mohanty (2002), Upscaling of soil hydraulic properties for steady state evaporation and infiltration, *Water Resour. Res.*, *38*(9), 1178, doi:10.1029/2001WR000704.

Zhu, J., and B. Mohanty (2003), Effective hydraulic parameters for steady state vertical flow in heterogeneous soils, *Water Resour. Res.*, *39*(8), 1227, doi:10.1029/2002WR001831.

E. D. Gutmann and E. E. Small, Department of Geological Sciences, University of Colorado, Boulder, CO 80309, USA. (gutmann@colorado.edu)